HHS Public Access

Author manuscript

J Neuroimaging. Author manuscript; available in PMC 2017 November 01.

Published in final edited form as:

J Neuroimaging. 2016 November ; 26(6): 626–634. doi:10.1111/jon.12354.

Assessment of glioma response to radiotherapy using multiple MRI biomarkers with manual and semi-automated segmentation algorithms

Yang Yu, **Dong-Hoon Lee**, **Shin-Lei Peng**, **Kai Zhang**, **Yi Zhang**, **Shanshan Jiang**, **Xuna Zhao**, **Hye-Young Heo**, **Xiangyang Wang**, **Min Chen**, **Hanzhang Lu**, **Haiyun Li**, and **Jinyuan Zhou**

Division of MR Research, Department of Radiology, Johns Hopkins University, Baltimore, MD (YY, DHL, SLP, KZ, YZ, SJ, XZ, HYH, XW, HL, HL, JZ); Department of Biomedical Engineering, Johns Hopkins University, Baltimore, MD (YY); Department of Radiology, Beijing Hospital, Beijing, China (XW, MC)

Abstract

Background and Purpose—Multi-modality MRI can provide complementary information in the assessment of brain tumors. We aimed to segment tumor in amide proton transfer-weighted (APTw) images and to investigate multi-parametric MRI biomarkers for the assessment of glioma response to radiotherapy. For tumor extraction, we evaluated a semi-automated segmentation method based on region of interest (ROI) results by comparing it with the manual segmentation method.

Methods—Thirteen nude rats injected with U87 tumor cells were irradiated by an 8-Gy radiation dose. All MRI scans were performed on a 4.7 T animal scanner pre-radiation, and at day 1, day 4, and day 8 post-radiation. Two experts performed manual and semi-automated methods to extract tumor ROIs on APTw images. Multi-modality MRI signals of the tumors, including structural (T_2 and T_1), functional (apparent diffusion coefficient and blood flow), and molecular (APTw and magnetization transfer ratio or MTR), were calculated and compared quantitatively.

Results—The semi-automated method provided more reliable tumor extraction results on APTw images than the manual segmentation, in less time. A considerable increase in the ADC intensities of the tumor was observed during the post-radiation. A steady decrease in the blood flow values and in the APTw signal intensities were found after radiotherapy.

Conclusions—The semi-automated method of tumor extraction showed greater efficiency and stability than the manual method. Apparent diffusion coefficient, blood flow, and APTw are all useful biomarkers in assessing glioma response to radiotherapy.

Keywords

Brain tumor; APT imaging; image segmentation; multiparametric MRI; response assessment

Corresponding Authors: Dr. Jinyuan Zhou, Ph.D., Division of MR Research, Department of Radiology, Johns Hopkins University School of Medicine, 600 N. Wolfe Street, 336 Park Building, Baltimore, MD 21287. jzhou@mri.jhu.edu; Phone: 410-955-7491; Fax: 410-614-1977.

Background and Purpose

Among the newly diagnosed primary brain tumors, gliomas account for 5 to 10 per 100,000 cases worldwide, with a median survival of 12 to 15 months for patients with glioblastoma.[1, 2] Because of the research performed by Walker in the 1970s, radiation therapy has become an effective method for the treatment of malignant gliomas, and can prolong patient survival.[3] Currently, MRI has been the most commonly used method to monitor the response of gliomas to treatment.[4, 5] As a powerful non-invasive tool, T_1-weighted (T_1w, with or without the use of gadolinium contrast agents) and T_2-weighted (T_2w, including fluid-attenuation inversion recovery or FLAIR) are the most widely used MRI sequences. However, there are still some limitations with these conventional MRI methods. First, gadolinium-based T_1w images may not distinguish tumor recurrence from radiation necrosis[6] or pseudoprogression.[7, 8] In addition, in case of pseudoresponse, the sudden disappearance of gadolinium enhancement during antiangiogenic therapy procedures prevents the detection of tumor recurrence.[8, 9] Therefore, tumor identification simply based on T_1w or T_2w images is not reliable clinically in every case.[10, 11]

Recently, more advanced MRI approaches for the detection of gliomas and their response to treatment have been proposed. For example, diffusion imaging with isotropic apparent diffusion coefficient (ADC) has widely been used for the discrimination of tumor and treatment effects in clinical protocols.[12–14] Perfusion imaging with blood flow and vascular permeability can provide crucial clues in the measurement of tumor activities.[15–18] In addition, it has been found that the conventional magnetization transfer (MT) imaging that reflects the semi-solid macromolecules in tissue[19] can provide additional information to MRI for the tumor assessment.[20, 21]

Amide proton transfer (APT) imaging is a newly developed MRI method that exploits the exchange between water protons and amide protons in mobile proteins and peptides in tissue.[22] By saturating these endogenous mobile protein and peptide amide protons, APT imaging detects a change in the free water signal intensity,[23, 24] leading to an endogenous contrast at the protein and peptide level. It is expected that the addition of APT or APT-weighted (APTw) images to the conventional and other advanced MRI methods would be more sensitive in evaluating the glioma response to therapy, potentially enabling a more accurate and predictable clinical assessment than the usage limited to the conventional and other advanced MRI sequences only.[25, 26] Additionally, the prediction accuracy can be further improved by more reliable approaches for region-of-interest (ROI) delineation. Indeed, the use of automatic or semi-automated methods for ROI determination has been implemented and developed. These algorithms significantly increase the accuracy of the localization of brain tumors and can achieve more stable extraction results.[27–31] Moreover, these methods reduce the processing time, compared to manual methods. The present study attempted to evaluate a semi-automated method for the ROI extraction on APTw images by comparing it with a manual segmentation by experts. With an experimental platform similar to that of our previous study[26], we present more explicit details for the assessment of glioma therapy response by quantitatively comparing different MRI parameters.

Methods

Rat Tumor Preparation

All experimental procedures were performed with the permission of Johns Hopkins Animal Care and Use Committee. In 13 T-cell deficient nude rats (20–22 weeks, 300–350 g), highly malignant anaplastic U87 gliomas were implanted inside the brain. During the tumor cell implantation, all rats were anesthetized through an intraperitoneal injection of solution (3–5 mL/kg) that contained ketamine hydrochloride (25 mg/mL) and xylazine (2.5 mg/mL). In order to set accurate and consistent positions, we first set a mark on the scalp incision that showed the sagittal and coronal sutures. Then, a needle was inserted into a burr hole that was made by an electric drill, positioned approximately 1 mm anterior to the coronal suture and 3 mm to the right of the sagittal suture. Next, at a depth of 5 mm from the skull, we injected each rat with U87 gliomas cells (one million in 4 μL media) over 3–4 min. Finally, we used wound clips to suture the rat skull. All rats underwent an MRI examination to determine the tumor side before the initial radiotherapy.

Radiotherapy

Eleven to 13 days after the tumor implantation, when the tumors grew to 4–6 mm in diameter on the T_2w images, all 13 rats were irradiated by a small-animal radiation research platform. The rat head and body were fixed with a special device during the whole procedure to avoid motion artifacts. All rats were anesthetized with 5% isoflurane, which lasted five minutes, and were kept in the 2–2.5% isoflurane environment in the subsequent radiotherapy. Then, with the guidance of an on-board, cone-beam CT image, well-collimated X-ray beams, with a dose of 8 Gy and an area of 10 × 10 mm^2, were administered to the center of the tumor. Similar to the reports in the literature,[32] a relatively low radiation dose was used in this study.

MRI Protocol

MR imaging was performed on a horizontal bore 4.7 T MR Imaging System (Bruker Biospin), pre-radiation, and at day 1, day 4, and day 8 post-radiation. Six quantitative MRI sequences were used with the following parameters: T_1 (inversion recovery; pre-delay = 3 s; echo time or TE = 30 ms; inversion recovery times = 0.05, 0.3,0.6,1.2, 1.8, 2.5, and 3.5 s; number of averages or NA = 4); T_2 (repetition time or TR = 3 s; TE = 30, 40, 50, 60, 70, 80, and 90 ms; NA = 4); isotropic ADC (TR = 3 s; TE = 80 ms; b-values = 0, 166.7, 333.3, 500, 666.7, 833.3, and 1000 s/mm^2; NA = 8); blood flow (arterial spin labeling or ASL; 3s labeling at a distance of 20 mm away from the imaging slice; TR = 6 s; TE = 28.6 ms); APT (radio-frequency saturation frequency offsets of ± 3.5 ppm; TR = 10 s; TE = 30 ms; saturation power = 1.3 μT; saturation time = 4 s; NA = 16); and MTR (radio-frequency saturation frequency offsets of 10 ppm (namely, 2 kHz at 4.7 T); TR = 10 s; TE = 30 ms; saturation power = 1.3 μT; saturation time = 4 s; NA = 16). All these sequences used single-shot, spin-echo, echo-planar imaging for image acquisition (single slice, field of view or FOV = 32 × 32 mm^2, matrix = 64 × 64). In addition, high-resolution T_2w images were acquired with the parameters of TR = 3 s, TE = 64 ms, thickness = 1.5 mm, NA = 2, FOV = 32 × 32 mm^2, and matrix = 192 × 192 in the coronal plane (or FOV = 42 × 32 mm^2, and matrix = 256 × 192 in the axial plane), with five slices overall. The follow-up MRI at a later

time point was always positioned at the same tumor location as the initial one, as much as possible, using intrinsic landmarks (corpus callosum, hippocampal commissure, and ventricles). As described in our previous studies[33], slab shimming around the image slice and adjustment of the scanner transmitter frequency (F0) were performed to reduce the B0 inhomogeneity effect on APTw images.

For the MRI scanning, all rats were anesthetized with 5% isoflurane in a mixture of 75% air and 25% oxygen for sedation, and then, breathed 1.5%–2.0% isoflurane through a nose cone. Rats in the magnet were monitored online through a small-animal respiratory gating system connected by a fiber optic cable, and the breathing rate of the animal was kept at 40 ± 5 breaths per minute by adjusting the isoflurane level. After the terminal MRI scanning, the animals were euthanized immediately using carbon dioxide inhalation, and the brains were stained with hematoxylin and eosin (H&E).

Image Analysis

An in-house script written in MATLAB (The MathWorks, Inc., Natick, MA) was used as the working environment for human–computer interactions. For a clear comparison result, T_1, T_2, and ADC maps were calculated as follows: $I = A + B\exp(-TI/T_1)$; $I = I_0\exp(-TE/T_2)$; and $I = I_0\exp(-b \times ADC)$. The CBF map was reconstructed from images with and without labeling, using previously described methods.[34] The APTw signal was calculated based on the difference of magnetization transfer ratio (MTR) values at ± 3.5 ppm relative to the water signal, namely, $MTR_{asym}(3.5\ ppm) = (S_{sat}(-3.5\ ppm) - S_{sat}(3.5\ ppm))/S_0$, where S_{sat} and S_0 are the signal intensities with and without radiofrequency irradiation. The MTR at 2 kHz was calculated using: $1 - S_{sat}(2\ kHz)/S_0$.

The ROIs in the tumor and in the tissue on the contralateral side of the brain were drawn by two reviewers (namely, Rater A and Rater B), who independently performed the manual and semi-automated methods, respectively, on the APTw images. Rater A and rater B had one- and four-year experience, respectively, in ROI drawing. The normal tissue on the contralateral side of the brain was used as a reference. Then, the mask of the drawn ROIs was transferred to other co-registered MR images. The lesions of the tumor that had shown abnormal MRI signals were mostly covered in the ROI areas, while the ventricles and peritumoral edema were not considered.

Manual Segmentation

The experts were asked to outline the margin of the tumor based on the APTw image for each rat, with the help from other types of MRI signals (especially ADC) when necessary. It has been demonstrated that the APTw image can separate tumor from peritumoral edema very well.[23, 35–37] The area of the contour derived from the APTw image was defined as the cross-sectional area of the tumor. Since the whole APTw hyperintense area was defined as the tumor, it may thus contain other components, including hemorrhage and cysts. The amount of time required for the manual segmentation was recorded.

Semi-automated Method

The semi-automated method was applied to the standard T_1w or T_2w image segmentation,[30, 38] and its use for the tumor ROI extraction based on the APTw image is not reported. The method began with the rough manual extraction in the tumor region. The experts outlined a possible ROI contour, which primarily include the APTw-hyperintense area, but may extend 2–3 mm outside from the irregular, blurred edge. Then, the original tumor mask was produced and automatically processed at the second stage. Based on the intensity difference between the APTw-hyperintense areas and normal brain tissue, entropy thresholding techniques[39] were used to identify the target ROI. In addition, the morphology process was implemented for image de-noising. The overall flowchart of the semi-automated method is shown in Fig 1.

Intra-rater and Inter-rater Reliability Trials

For the intra-rater reliability trials, the second time measurements for both the manual and semiautomated methods were conducted one week after the first measurement. To perform the inter-rater reliability trials with the semi-automated method, both the raters were trained in a 10-minute session to familiarize themselves with the test procedure. This session was about the introduction to the interface program and the emphasis conveyed to the raters about pointing out the blurred areas of the ROI. Then, Rater A and Rater B independently implemented both manual and semi-automated determinations of the ROIs.

Statistical Analysis

The results from all MR images were described as mean ± SD. The tumor areas obtained from APTw images were assessed with the intra-rater and inter-rater reliability described by Bland-Altman[40] and the mean with ± 2 SD was labeled in the figures. Based on the calculation of differences against the mean, the agreement between the two sets of mechanisms was then examined by a two-tailed t-test. The differences in tumor areas at several different time points were analyzed by a one-way analysis of variance test, followed by the Turkey test. All statistical analyses were performed using the SPSS software (Version 18, Chicago, IL). The level of significance was set at $p < 0.05$.

Results

Semi-automated Method

To assess the semi-automated and manual methods, we evaluated the inter-rater and intra-rater reliability of ROI extraction. At first, all tumor masks required an initial boundary condition. The most frequent errors were due to suboptimal brain extraction that was caused, for example, by the blurred areas, especially the transition areas close to the ROI. For the edges with a high contrast ratio, even if there were many details and irregularities, the contour could be drawn broadly. The mean time for the initial condition determination was 45 s (ranging from 5 s to 1 min) per scan. The subsequent automated step of the tumor mask generation required 20 s of computer time with a regular desktop computer (2.90 GHz CPU, 8 GB RAM). Therefore, the overall average time required to produce a single tumor mask was about one minute. The reviewer recorded a time of five minutes for the manual method,

per examination, which also included the incorrect drawing and reproduction time (since the manual method required more detailed detections, causing a greater chance of retesting due to mistakes).

Intra-rater Reliability Trial

For both the manual and semi-automated methods, the second time measurements were conducted one week after the first measurements. There was a slight but significant difference in Test 1 (manual method) measurements for rater A ($p_1 = 0.0161$), while Test 2 (semi-automated method) measurements ($p_2 = 0.7081$) showed no significant difference. The test results are shown in Fig 2A and B.

Even considering personal bias, or sight and hand vibration errors at different periods, the agreement between the two ratings was fair to good by visual estimation of the figs. The collected data were mainly distributed near the midline of the y-axis (difference against the mean). This indicates that the same person tended to give similar results at different times, leading to more stable ROI extraction results.

Inter-rater Reliability Trial

Rater A and Rater B independently performed both manual and semi-automated determinations of the ROIs. The manual method had a more scattered distribution, as shown in Fig 2C and D by estimation. The p values also showed that, using the manual method, the two raters produced significantly different ($p = 0.0000$) results, while the results using the semi-automated method were stable ($p = 0.1464$).

Given the potential personal bias, or sight and hand vibration errors from different raters, the agreement between the semi-automated ratings was fair to good. The data distributed near the midline of the y-axis indicated that this method remained stable when the ROI was drawn by different people. When the inter-rater reliability was assessed, the manual method was more prone to personal bias and errors, leading to unstable results for the ROI. Even if the raters demonstrated the same detection and judgment of the ROI boundary, there could still be different conclusions about the areas because of manual drawing errors.

Morphological Features of Irradiated Tumors

The tumors had grown to 4–6 mm in diameter pre-radiotherapy (at 11–13 days post-implantation). The T_2w MRI revealed that, after 8 Gy radiation therapy, all rat tumors were still growing in size during the subsequent examinations, as shown in Fig 3A. The transition of the tumor cross-sectional areas obtained from the APTw images for all the rats is shown in Fig 3B. At day 4 and day 8 post-radiotherapy, the tumor sizes showed significant increases ($p < 0.001$).

Multi-modality MRI Signals of Irradiated Tumors

Fig 4A shows the multi-modality MRI signal features for one representative rat. On the T_1 maps, T_2 maps, ADC maps, and APTw images, the tumor was hyperintense, compared with the normal tissue on the contralateral side of the brain, while it was hypointense on the MTR maps. Imperceptible changes on T_1, T_2, and MTR maps throughout the time points can be

detected. Notably, on the ADC maps, blood flow maps, and APTw images, visual differences can be observed between pre-radiotherapy and post-radiotherapy. On the blood flow maps, both the tumor and contralateral part of the normal brain tissue had clear signal intensities. The tumor demonstrated minor hyperintensity or hypointensity at pre-radiation, which changed to hypointensity at post-radiation. On the ADC maps, the intensity of the tumor region increased at post-radiation time points, leading to a clear contrast with respect to the contralateral part of the normal brain tissue. On the APTw images, the signal intensity overall showed a decrease in post-radiation observations, similar to that of the blood flow. The H&E histological section at 8 days post-radiation showed the presence of coagulative necrosis in the irradiated tumor.

Histogram Analysis

The histograms in Fig 5 show the multi-parametric MRI values of one irradiated rat, which describes the status and size change of the tumors. After irradiation, the tumor continued to increase in size, and the histograms became larger and shifted. For instance, the ADC indicated a right shift after radiation therapy, just as noted previously.[25, 26] In contrast, the peaks of blood flow and APTw histograms had a steady left shift after irradiation. The other three histograms, T_1, T_2, and MTR, however, did not show a distinct change from pre-radiation to post-radiation.

Discussion

Pathological analysis of a tumor is the only reliable method with which to assess the tumor response to ongoing treatments. However, tissue sampling via biopsy is not feasible for all brain regions. More reliable imaging parameters that may improve the clinical diagnosis, including perfusion and diffusion, have been proposed, as mentioned previously. Earlier studies have suggested that APTw can yield different signals for malignant tumors and peritumoral edema, as well as high-grade and low-grade gliomas.[35–37, 41] These findings stem from the fact that the APTw signals are primarily associated with the cellular proteins and peptides in tissue, which are different in tumor as opposed to the tissue in the normal contralateral side of the brain.[42, 43] The fact that the APTw signals are sensitive to mobile protein changes in tumor indicates that APTw can provide prognostic information and reliable assessments of tumor after radiation treatments. It has been suggested that APTw signals are hypointense in the necrotic area of tumor regions while the actively growing areas are hyperintense.[25, 26] Based on this, we could assume that the APTw drop inside the tumor region post-treatment represent necrosis from the radiation.[44, 45] In this regard, we would like to note that the presence of spontaneous necrosis typically observed in malignant gliomas may be a confounder for radiation necrosis, as spontaneous necrosis also shows a low APTw signal.

A recent study revealed that the more standardized and widely available volumetric MR imaging data not only provide detailed information about tumor detection and treatment assessment, but also the means to incorporate volumetric measurements.[46] Since the tumors in that study were not subject to pathologic analysis, the ultimate accuracy of the investigation for the ROI on an APTw image is yet to be determined. However, in our study,

during the performance of the semi-automated method, the low inter-observer variability reflected a close agreement between different experts. By comparing these results to the manual results, we concluded that the accuracy of the semi-automated method is not inferior to that of the experts. The semi-automated method matched the expert judgment on the ROI extractions. As stated earlier, the manual segmentation is time-consuming and the inter-rater variability is considerably high. Therefore, the automatic or semi-automated methods for tumor ROI extraction would be potentially superior, because they have been studied in other organs with promising results.[47] There are many literature reports on automatic brain tumor segmentation based on T_1w or T_2w.[48, 49] especially the widely used voxel-based fuzzy clustering methods[50, 51]. For APTw images, the fusion may cause minor clusters due to the change in topology. Similar to the method used by Chow et al.,[52] the semi-automated method relies on the human-computer interface at the first step of ROI editing, in order to define the initial mask by roughly drawing the contour of the enclosed tumor. This is the only step that relies on interactions with the radiologists. The semi-automated process is considerably faster than the manual method (one minute vs. five minutes), which, unavoidably, depends on the experience of the radiologist. Importantly, intra-rater reliability was excellent for the semi-automated method, as demonstrated by its good convergence validity, but test-retest reliability over an interval of 10 days was lower than what the manual method provided. The reason of this strength in the semi-automated method is that, during the editing process, the manual method can hardly match an associated contour of the tumor region. An alternative approach to reduce the inter-rater variability has been proposed.[46] However, the limitation regarding treatment-induced changes when determining the ROI in this study is unavoidable. For our time-dependent MRI multiparameter collection, we are more likely to reach similar conclusions about the contour for uniform subjects, with high reproducibility, using the semi-automated method. The inter-rater reliability study for the two methods revealed that the semi-automated method would be more homogeneous in contrast than the manual method. This criteria-based method will help radiologists reach a stable result for the ROI extraction. An accurate ROI decision is important not only for volume estimation *in vivo* when assessing tumor treatments, but is also crucial for perfusion, diffusion, and other MRI parameter calculations based on the ROI. Further standardization of the decisions about the margins of fusion areas is highly desirable for ROI segmentation.

It has been widely believed that the changes in tumor ADC values following the treatment are associated with treatment effects in the past two decades.[53–55] ADC values are a rough measure of the magnitude of water molecule diffusion, reflecting the cell density reduction and water mobility. In a pathological process, the increased ADC values relative to the normal brain tissue may be caused by tumor growth, edema, and necrosis. In irradiated subjects, most studies have reported higher ADC values were attributable to the apoptotic and/or necrotic processes. Fig 5 shows that ADC values have a durable right shift during tumor development, after radiation therapy, except that at day 4 they remained consistent with those at day 1. Our results for ADC change agreed with previous studies.[26] Moreover, in some cases of unchanged or lower ADC values, the radiation-induced effects, including gliosis, fibrosis, macrophage invasion, vascular changes, and demyelization, may be a possible explanation.

The ASL technology has been used to quantify tumor blood flow. Figs 4 and 5 show that, for both tumor region and the contralateral normal brain tissue, blood flow signals on ROI simultaneously decreased, on average, in all post-radiation stages. As showed previously,[25, 26] the reduction of blood flow signals also occurred in non-treated rats. This might be attributable to the high intracranial pressure due to the large tumor in an advanced stage of tumor growth, which needs to be confirmed by further investigation. The dynamic, susceptibility-weighted, contrast-enhanced (DSC) MRI technique has a shorter scan time and lower standard deviations than the ASL method.[56] However, ASL MRI is non-invasive and also clearly differentiates recurrent tumor from radiation necrosis in patients with gliomas.[57, 58] This is particularly meaningful in the clinical treatment of patients, since ASL MRI as well as APT use endogenous contrast agents and avoid intravenous injection, which is potentially problematic for pediatric cases. Compared with diffusion ADC maps, APTw and perfusion blood flow have lower signal-to-noise ratios. Thus, combining the information from perfusion, diffusion, and APTw with conventional imaging methods would likely provide a more detailed and accurate picture to be analyzed in clinical treatments. More insightful research on these topics, along with standardized criteria, is needed in the future.

There are a few limitations to our study. First, we did not establish a non-irradiated rat group as a control to compare the tumor development at different periods. We did also not follow the survival rate after the last MR image was obtained. Therefore, we could not determine the treatment efficacy of low-dose radiation (8 Gy), although it is already known that the dose and exposure time are critical for radiation effects.[3, 59] Second, our ROI extraction of the tumor location relied on expert editing to evaluate the accuracy, while the objective position of the tumor should be analyzed by pathology.

Conclusions

The semi-automated method of ROI extraction, based on APTw images, is more expeditious than the manual segmentation. With regard to the inter-rater and intra-rater reliability, the semi-automated method allows the radiologist to provide a lower standard deviation, thus arriving at a more stable conclusion about contour. This method is helpful in determining perfusion and APT MRI parameters on the ROI extraction. Our results show that the ADC, blood flow, and APTw parameters are all helpful MRI parameters in distinguishing tumor recurrence from treatment-related necrosis. ADC and APTw are more sensitive than blood flow. Meanwhile, protein-based APTw images are non-invasive and sensitive to post-radiation therapy assessment. More criteria for ROI detection and a determination of the accuracy of multiparametric MRI necessitate further study in the near future.

Acknowledgments

The authors thank Ms. Mary McAllister for editorial assistance. This work was supported in part by grants from the National Institutes of Health (R01EB009731, R01CA166171, R01NS083435, and R21EB015555) and the National Natural Science Foundation of China (81361120392).

References

1. Legler JM, Ries LA, Smith MA, et al. Cancer surveillance series [corrected]: brain and other central nervous system cancers: recent trends in incidence and mortality. J Natl Cancer Inst. 1999; 91:1382–90. [PubMed: 10451443]
2. Wen PY, Kesari S. Malignant gliomas in adults. N Engl J Med. 2008; 359:492–507. [PubMed: 18669428]
3. Walker MD, Strike TA, Sheline GE. An analysis of dose-effect relationship in the radiotherapy of malignant gliomas. Int J Radiat Oncol Biol Phys. 1979; 5:1725–31. [PubMed: 231022]
4. Macdonald DR, Cascino TL, Schold SC Jr, Cairncross JG. Response criteria for phase II studies of supratentorial malignant glioma. J Clin Oncol. 1990; 8:1277–80. [PubMed: 2358840]
5. Wen PY, Macdonald DR, Reardon DA, et al. Updated response assessment criteria for high-grade gliomas: response assessment in neuro-oncology working group. J Clin Oncol. 2010; 28:1963–72. [PubMed: 20231676]
6. Eyster EF, Nielsen SL, Sheline GE, Wilson CB. Cerebral radiation necrosis simulating a brain tumor. Case report J Neurosurg. 1974; 40:267–71. [PubMed: 4203210]
7. Brandsma D, Stalpers L, Taal W, Sminia P, van den Bent MJ. Clinical features, mechanisms, and management of pseudoprogression in malignant gliomas. Lancet Oncol. 2008; 9:453–61. [PubMed: 18452856]
8. Brandsma D, van den Bent MJ. Pseudoprogression and pseudoresponse in the treatment of gliomas. Curr Opin Neurol. 2009; 22:633–8. [PubMed: 19770760]
9. Hicklin DJ, Ellis LM. Role of the vascular endothelial growth factor pathway in tumor growth and angiogenesis. J Clin Oncol. 2005; 23:1011–27. [PubMed: 15585754]
10. Hasso A, Kortman K, Bradley W. Supratentorial neoplasms. Magnetic resonance imaging. 1992; 1:770–817.
11. Hicks R, Edelman R, Hesselink J, Zlatkin M. Supratentorial brain tumors. Clinical magnetic resonance imaging. 1996; 1:533–56.
12. Maier SE, Bogner P, Bajzik G, et al. Normal brain and brain tumor: multicomponent apparent diffusion coefficient line scan imaging. Radiology. 2001; 219:842–9. [PubMed: 11376280]
13. Kono K, Inoue Y, Nakayama K, et al. The role of diffusion-weighted imaging in patients with brain tumors. AJNR Am J Neuroradiol. 2001; 22:1081–8. [PubMed: 11415902]
14. Yamasaki F, Kurisu K, Satoh K, et al. Apparent diffusion coefficient of human brain tumors at MR imaging. Radiology. 2005; 235:985–91. [PubMed: 15833979]
15. Senger DR, Galli SJ, Dvorak AM, Perruzzi CA, Harvey VS, Dvorak HF. Tumor cells secrete a vascular permeability factor that promotes accumulation of ascites fluid. Science. 1983; 219:983–5. [PubMed: 6823562]
16. Taylor DG, Bushell MC. The spatial mapping of translational diffusion coefficients by the NMR imaging technique. Phys Med Biol. 1985; 30:345–9. [PubMed: 4001161]
17. Ostergaard L, Hochberg FH, Rabinov JD, et al. Early changes measured by magnetic resonance imaging in cerebral blood flow, blood volume, and blood-brain barrier permeability following dexamethasone treatment in patients with brain tumors. J Neurosurg. 1999; 90:300–5. [PubMed: 9950501]
18. Covarrubias DJ, Rosen BR, Lev MH. Dynamic magnetic resonance perfusion imaging of brain tumors. Oncologist. 2004; 9:528–37. [PubMed: 15477637]
19. Wolff SD, Balaban RS. Magnetization transfer contrast (MTC) and tissue water proton relaxation in vivo. Magn Reson Med. 1989; 10:135–44. [PubMed: 2547135]
20. Gong QY, Eldridge PR, Brodbelt AR, et al. Quantification of tumour response to radiotherapy. Br J Radiol. 2004; 77:405–13. [PubMed: 15121704]
21. Garcia M, Gloor M, Bieri O, et al. Imaging of primary brain tumors and metastases with fast quantitative 3-dimensional magnetization transfer. J Neuroimaging. 2015; 25:1007–14. [PubMed: 25702714]
22. Zhou JY, Payen JF, Wilson DA, Traystman RJ, van Zijl PCM. Using the amide proton signals of intracellular proteins and peptides to detect pH effects in MRI. Nature Medicine. 2003; 9:1085–90.

23. Zhou JY, Lal B, Wilson DA, Laterra J, van Zijl PCM. Amide proton transfer (APT) contrast for imaging of brain tumors. Magnetic Resonance in Medicine. 2003; 50:1120–6. [PubMed: 14648559]
24. Jones CK, Schlosser MJ, van Zijl PCM, Pomper MG, Golay X, Zhou JY. Amide proton transfer imaging of human brain tumors at 3T. Magnetic Resonance in Medicine. 2006; 56:585–92. [PubMed: 16892186]
25. Zhou J, Tryggestad E, Wen Z, et al. Differentiation between glioma and radiation necrosis using molecular magnetic resonance imaging of endogenous proteins and peptides. Nature Med. 2011; 17:130–4. [PubMed: 21170048]
26. Hong XH, Liu L, Wang MY, et al. Quantitative multiparametric MRI assessment of glioma response to radiotherapy in a rat model. Neuro-Oncology. 2014; 16:856–67. [PubMed: 24366911]
27. Lee, J-D.; Lee, J-Y.; Hsiao, Y-L. A wavelet-based approach to detect bladder tumor in color images. TENCON 99 Proceedings of the IEEE Region 10 Conference; 1999; p. 597-600.
28. Tang H, Wu EX, Ma QY, Gallagher D, Perera GM, Zhuang T. MRI brain image segmentation by multi-resolution edge detection and region selection. Computerized Medical Imaging and Graphics. 2000; 24:349–57. [PubMed: 11008183]
29. Kaus MR, Warfield SK, Nabavi A, Black PM, Jolesz FA, Kikinis R. Automated segmentation of MR images of brain tumors. Radiology. 2001; 218:586–91. [PubMed: 11161183]
30. Ho, S.; Bullitt, E.; Gerig, G. Level-set evolution with region competition: Automatic 3-D segmentation of brain tumors. 16th International Conference on Pattern Recognition, Vol I, Proceedings; 2002; p. 532-5.
31. Badran, EF.; Mahmoud, EG.; Hamdy, N. An Algorithm for Detecting Brain Tumors in MRI Images. Icces'2010: The 2010 International Conference on Computer Engineering & Systems; 2010; p. 368-73.
32. Hadaczek P, Ozawa T, Soroceanu L, et al. Cidofovir: a novel antitumor agent for glioblastoma. Clin Cancer Res. 2013; 19:6473–83. [PubMed: 24170543]
33. Wang M, Hong X, Chang CF, et al. Simultaneous detection and separation of hyperacute intracerebral hemorrhage and cerebral ischemia using amide proton transfer MRI. Magn Reson Med. 2015; 74:42–50.
34. Williams DS, Detre JA, Leigh JS, Koretsky AP. Magnetic resonance imaging of perfusion using spin inversion of arterial water. Proc Natl Acad Sci U S A. 1992; 89:212–6. [PubMed: 1729691]
35. Zhou JY, Blakeley JO, Hua J, et al. Practical data acquisition method for human brain tumor amide proton transfer (APT) imaging. Magnetic Resonance in Medicine. 2008; 60:842–9. [PubMed: 18816868]
36. Wen Z, Hu S, Huang F, et al. MR imaging of high-grade brain tumors using endogenous protein and peptide-based contrast. NeuroImage. 2010; 51:616–22. [PubMed: 20188197]
37. Zhou JY, Zhu H, Lim M, et al. Three-Dimensional Amide Proton Transfer MR Imaging of Gliomas: Initial Experience and Comparison With Gadolinium Enhancement. Journal of Magnetic Resonance Imaging. 2013; 38:1119–28. [PubMed: 23440878]
38. Odland A, Server A, Saxhaug C, et al. Volumetric glioma quantification: comparison of manual and semi-automatic tumor segmentation for the quantification of tumor growth. Acta Radiol. 2014
39. Chang CI, Du Y, Wang J, Guo SM, Thouin PD. Survey and comparative analysis of entropy and relative entropy thresholding techniques. Iee Proceedings-Vision Image and Signal Processing. 2006; 153:837–50.
40. Bland JM, Altman DG. Statistical Methods for Assessing Agreement between Two Methods of Clinical Measurement. Lancet. 1986; 1:307–10. [PubMed: 2868172]
41. Togao O, Yoshiura T, Keupp J, et al. Amide proton transfer imaging of adult diffuse gliomas: correlation with histopathological grades. Neuro-Oncology. 2014; 16:441–8. [PubMed: 24305718]
42. Hobbs SK, Shi G, Homer R, Harsh G, Atlas SW, Bednarski MD. Magnetic resonance image-guided proteomics of human glioblastoma multiforme. J Magn Reson Imaging. 2003; 18:530–6. [PubMed: 14579395]
43. Howe FA, Barton SJ, Cudlip SA, et al. Metabolic profiles of human brain tumors using quantitative in vivo H-1 magnetic resonance spectroscopy. Magnetic Resonance in Medicine. 2003; 49:223–32. [PubMed: 12541241]

44. Wang SL, Tryggestad E, Zhou TT, et al. Assessment of MRI Parameters as Imaging Biomarkers for Radiation Necrosis in the Rat Brain. International Journal of Radiation Oncology Biology Physics. 2012; 83:E431–E6.
45. Sagiyama K, Mashimo T, Togao O, et al. In vivo chemical exchange saturation transfer imaging allows early detection of a therapeutic response in glioblastoma. Proc Natl Acad Sci (USA). 2014; 111:4542–7. [PubMed: 24616497]
46. Sorensen AG, Batchelor TT, Wen P, Zhang WT, Jain RK. Response criteria for glioma. Nature Clinical Practice Oncology. 2008; 5:634–44.
47. Mozley PD, Bendtsen C, Zhao BS, et al. Measurement of Tumor Volumes Improves RECIST-Based Response Assessments in Advanced Lung Cancer. Translational Oncology. 2012; 5:19–25. [PubMed: 22348172]
48. Balafar MA, Ramli AR, Saripan MI, Mashohor S. Review of brain MRI image segmentation methods. Artificial Intelligence Review. 2010; 33:261–74.
49. Llado X, Oliver A, Cabezas M, et al. Segmentation of multiple sclerosis lesions in brain MRI: A review of automated approaches. Information Sciences. 2012; 186:164–85.
50. Vaidyanathan M, Clarke LP, Hall LO, et al. Monitoring brain tumor response to therapy using MRI segmentation. Magnetic Resonance Imaging. 1997; 15:323–34. [PubMed: 9201680]
51. Corso JJ, Sharon E, Dube S, El-Saden S, Sinha U, Yuille A. Efficient multilevel brain tumor segmentation with integrated Bayesian model classification. Ieee Transactions on Medical Imaging. 2008; 27:629–40. [PubMed: 18450536]
52. Chow DS, Qi J, Guo X, et al. Semiautomated Volumetric Measurement on Postcontrast MR Imaging for Analysis of Recurrent and Residual Disease in Glioblastoma Multiforme. American Journal of Neuroradiology. 2014; 35:498–503. [PubMed: 23988756]
53. Chenevert TL, McKeever PE, Ross BD. Monitoring early response of experimental brain tumors to therapy using diffusion magnetic resonance imaging. Clin Cancer Res. 1997; 3:1457–66. [PubMed: 9815831]
54. Bulakbasi N, Kocaoglu M, Ors F, Tayfun C, Ucoz T. Combination of single-voxel proton MR spectroscopy and apparent diffusion coefficient calculation in the evaluation of common brain tumors. American Journal of Neuroradiology. 2003; 24:225–33. [PubMed: 12591638]
55. Bulakbasi N, Guvenc I, Onguru O, Erdogan E, Tayfun C, Ucoz T. The added value of the apparent diffusion coefficient calculation to magnetic resonance imaging in the differentiation and grading of malignant brain tumors. J Comput Assist Tomogr. 2004; 28:735–46. [PubMed: 15538145]
56. Essig M, Shiroishi MS, Nguyen TB, et al. Perfusion MRI: The Five Most Frequently Asked Technical Questions. American Journal of Roentgenology. 2013; 200:24–34. [PubMed: 23255738]
57. Law M, Young RJ, Babb JS, et al. Gliomas: Predicting time to progression or survival with cerebral blood volume measurements at dynamic susceptibility-weighted contrast-enhanced perfusion MR imaging. Radiology. 2008; 247:490–8. [PubMed: 18349315]
58. Hu LS, Eschbacher JM, Heiserman JE, et al. Reevaluating the imaging definition of tumor progression: perfusion MRI quantifies recurrent glioblastoma tumor fraction, pseudoprogression, and radiation necrosis to predict survival. Neuro-Oncology. 2012; 14:919–30. [PubMed: 22561797]
59. Merchant TE, Hua CH, Shukla H, Ying X, Nill S, Oelfke U. Proton versus photon radiotherapy for common pediatric brain tumors: comparison of models of dose characteristics and their relationship to cognitive function. Pediatr Blood Cancer. 2008; 51:110–7. [PubMed: 18306274]

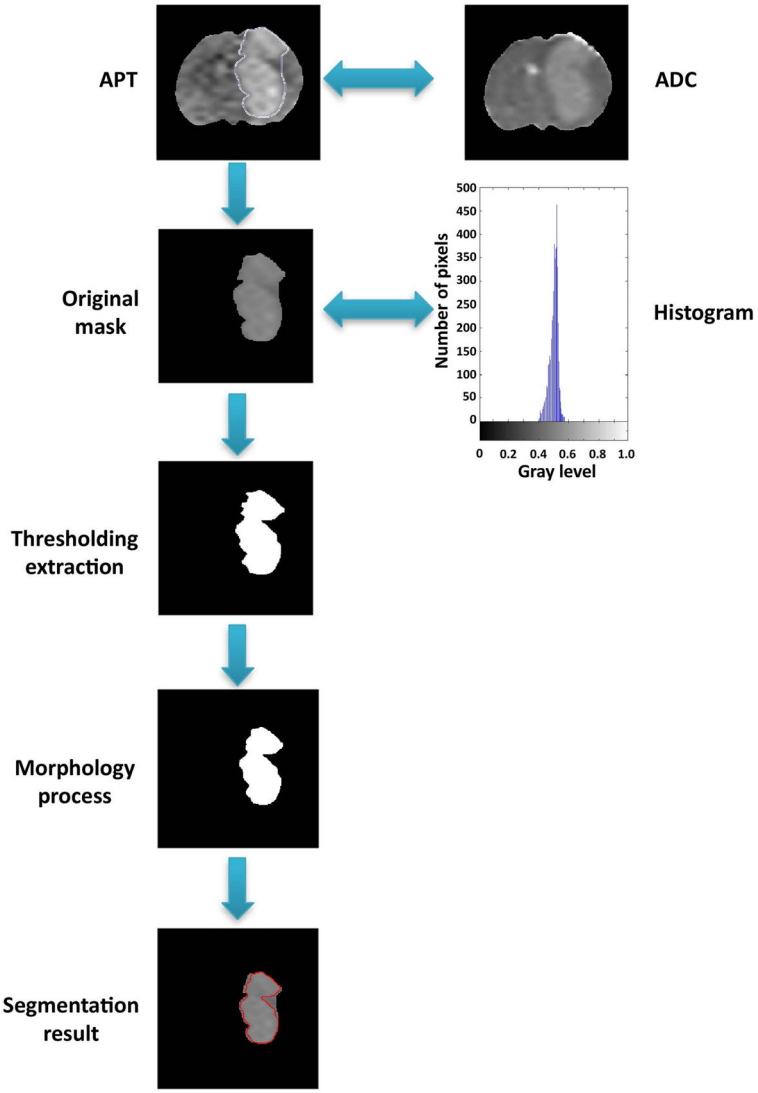

Fig. 1.

Flow-chart of the semi-automated tumor region extraction method for one sample. First, an initial ROI was extracted by the human interaction from an APTw map. If necessary, the information was co-registered to the ADC map. Second, the histogram was taken into consideration and the original mask was labeled. Next, the temporary result was de-noised by a morphologic process. Finally, the contour was highlighted.

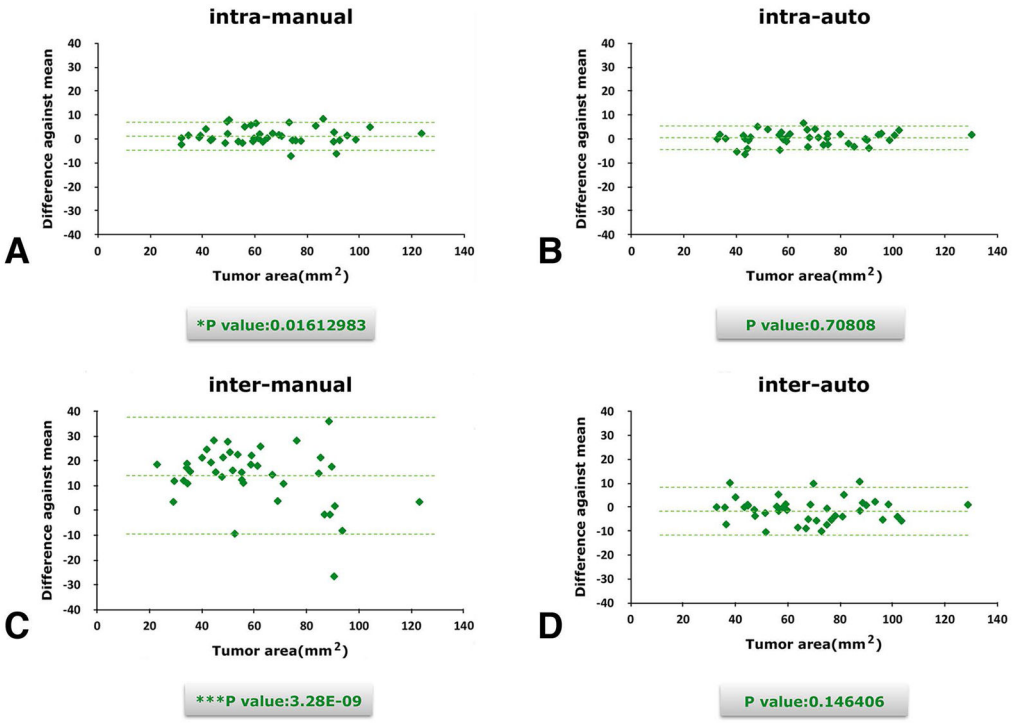

Fig. 2.

Intra-rater (A and B) and inter-rater (C and D) analysis comparison between manual and semiautomated ROI extraction. This demonstrates that manual segmentation had a wider distribution than the semi-automated method in both inter- and intra-rater experiments.

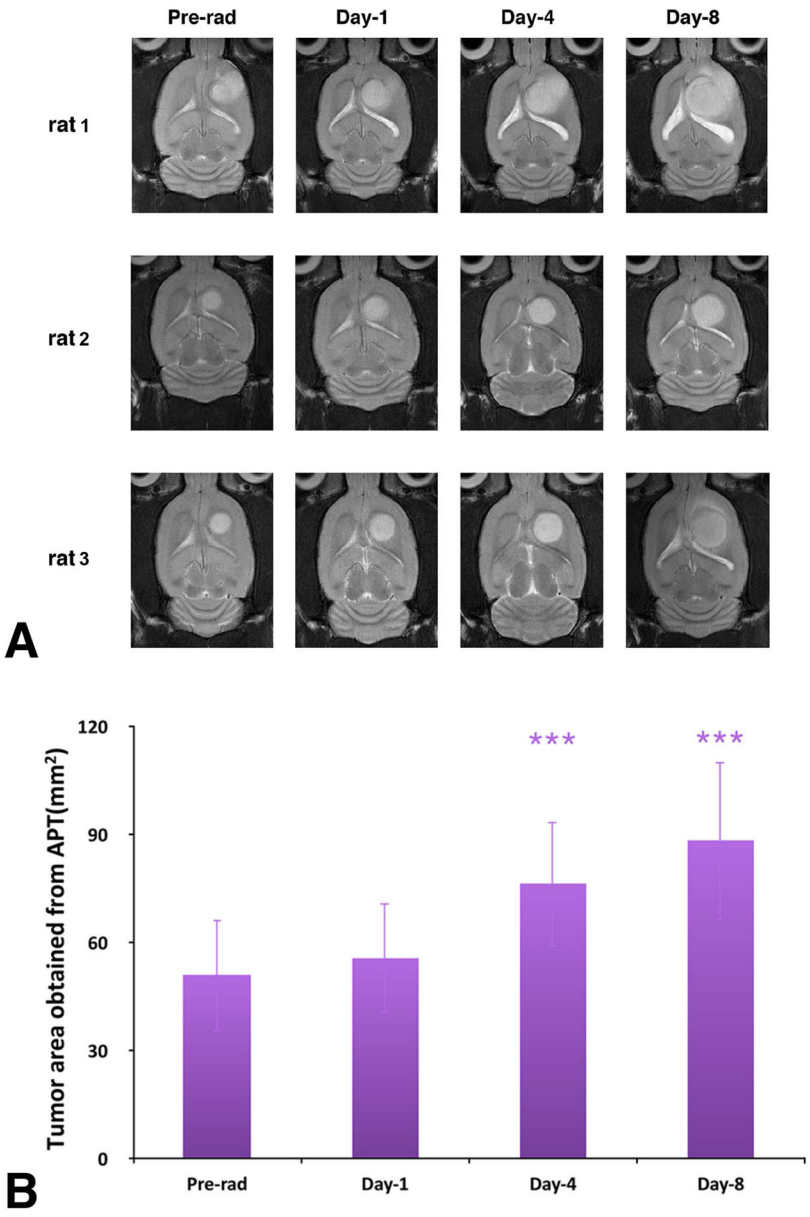

Fig. 3.

(A) T_2w MRI features investigated at different time points of pre-radiotherapy and on day 1, day 4, and day 8 post-radiotherapy for three different rats. The irradiated tumors were still growing during the postradiation development. (B) Tumor cross-section areas obtained from the APTw images at different time points of pre-radiation and on day 1, day 4, and day 8 postradiation. The statistical significance of the difference compared with pre-radiation: ***$p < 0.001$.

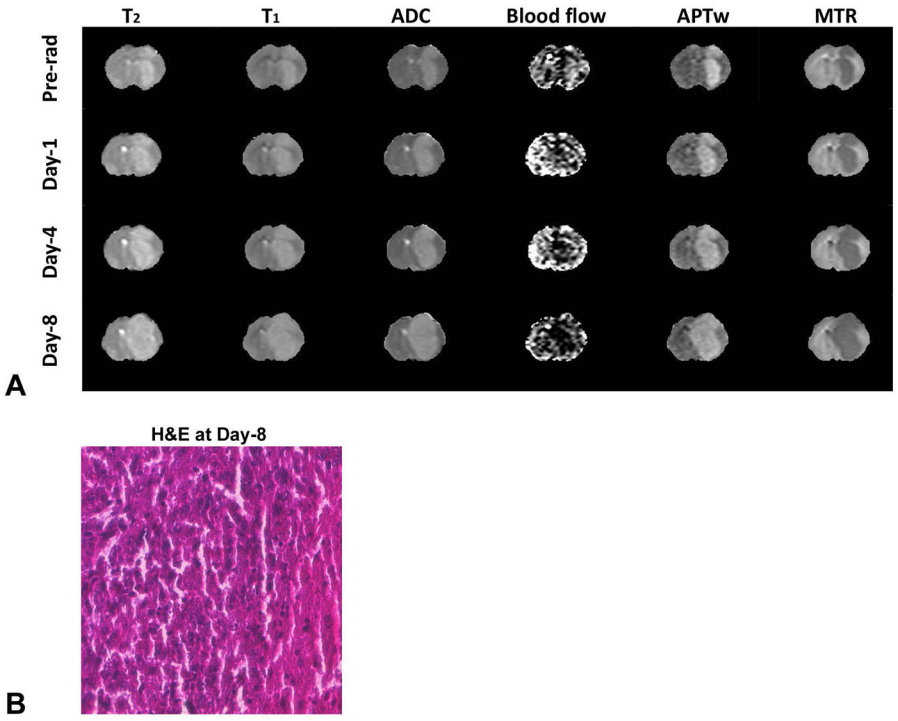

Fig. 4.

(A) Changes in T_2 maps (0 – 100 ms), T_1 maps (0.5 – 2 s), ADC maps (0 – 2×10^{-9} m^2/s), blood flow maps (0 – 200 mL/100 g/min), APTw images (−10% to 10% of the bulk water signal intensity), and MTR maps at 2 kHz (0% – 50% of the bulk water signal intensity) at different time points of pre-radiation and on day 1, day 4, and day 8 post-radiation for one representative rat with a U87 MG glioma. The outside noise of brain tissue has been filtered out. (B) The H&E image at 8 days post-radiation, taken from the central part of the tumor.

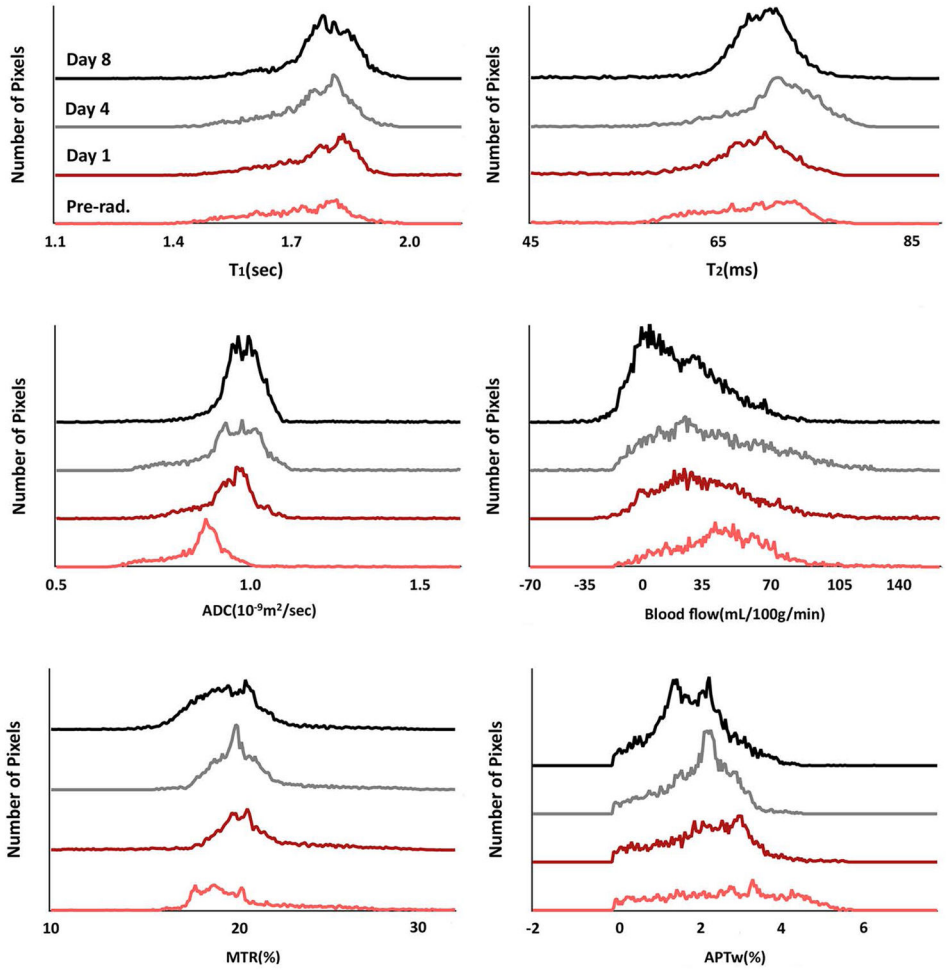

Fig. 5.

Histogram analysis of multiparametric MRI biomarkers at different time points of pre-radiation and on day 1, day 4, and day 8 postradiation for U87 MG glioma in a rat. The ADC histogram had a right shift, while blood flow signals and APTw intensity had a left shift after radiotherapy.